Molecular correlation functions for uniaxial ellipsoids in the isotropic state

Cristiano De Michele[a)]
Dipartimento di Fisica and INFM-CRS Soft, Universitá di Roma "La Sapienza," Piazzale Aldo Moro 2, 00185 Roma, Italy

Antonio Scala
Dipartimento di Fisica and INFM-CRS SMC, Universitá di Roma "La Sapienza," Piazzale Aldo Moro 2, 00185 Roma, Italy

Rolf Schilling
Johannes-Gutenberg-Universitat Mainz, D-55099 Mainz, Germany

Francesco Sciortino
Dipartimento di Fisica and INFM-CRS Soft, Universitá di Roma "La Sapienza," Piazzale Aldo Moro 2, 00185 Roma, Italy

We perform event-driven molecular dynamics simulations of a system composed by uniaxial hard ellipsoids for different values of the aspect ratio and packing fraction. We compare the molecular orientational-dependent structure factors previously calculated within the Percus-Yevick approximation with the numerical results. The agreement between theoretical and numerical results is rather satisfactory. We also show that, for specific orientational quantities, the molecular structure factors are sensitive to the particle shape and can be used to distinguish prolate from oblate ellipsoids. A first order theoretical expansion around the spherical shape and a geometrical analysis of the configurations confirms and explains such an observation. © *2006 American Institute of Physics*. [DOI: 10.1063/1.2176679]

I. INTRODUCTION

The structure of *simple* liquids can be characterized by the density-density correlator $g(r)$ or by its Fourier transform, the static structure factor $S(q)$. Strong efforts have been made to derive analytical tools for the calculation of these quantities, since $g(r)$ or $S(q)$ allows one to calculate several thermodynamical quantities, e.g., the equation of state. Among the most prominent theoretical approaches are the Percus-Yevick (PY), the hypernetted chain (HNC), and other more elaborate integral equations.[1] For models of simple liquids—when the number density ρ is not too large—integral equations provide predictions for $g(r)$ and $S(q)$ which well reproduce the "exact" results evaluated from experiments or simulations.

For *molecular* liquids, structural information become more diverse due to the presence of the orientational degrees of freedom and of their interactions with the translational ones. Expansion of the angular dependent microscopic density with respect to spherical harmonics and Wigner functions for linear and arbitrary molecules, respectively, leads to a generalization of $S(q)$ to tensorial correlators $S_{\lambda\lambda'}(\mathbf{q})$ (see Sec. II B). Several analytical approaches have been proposed to calculate these correlation functions. The simplest one performs *Ansätze* which relates $S_{\lambda\lambda'}(\mathbf{q})$, or the corresponding direct correlation function $c_{\lambda\lambda'}(\mathbf{q})$, to $S(q)$ or $c(q)$, $q=|\mathbf{q}|$ of an appropriately chosen related simple liquid.[2–9] Similar to this is the *Ansatz* for $c_{\lambda\lambda'}(\mathbf{q})$ based on the geometry of two

molecules.[10–12] The thermodynamical perturbation theory is a systematic approach which uses a liquid system of *isotropic* particles as a reference and considers the deviation of the particles from *sphericity* as a perturbation. Different types of expansions exist, depending on the quantity which is expanded. For more details the reader may consult Ref. 13. Finally, the integral equation theories have been extended to molecular liquids.[1,13]

As compared to simple liquids, the quality of the integral equations for anisotropic particles has been less intensively investigated. Furthermore, comparisons have been mainly restricted to hard ellipsoids of revolution and to the value of the coefficients $g_{ll'm}(r)$ and $c_{ll'm}(r)$ of the expansion into rotational invariants of, respectively, the pair distribution and direct correlation function in real space. The quality of PY and HNC theories for a liquid of hard ellipsoids[14] has been tested against molecular dynamic simulation data 15 years ago.[15] Reference 14 reports such a comparison together with earlier Monte Carlo (MC) results,[16] however, restricted to the center of mass correlator $g_{000}(r)$. Satisfactory agreement has been found for both approximation schemes. The PY theory seems to be inferior to HNC theory, because (i) the PY correlators for *oblate* ellipsoids deviate stronger than the HNC correlation from the corresponding molecular dynamics (MD) results and (ii) PY theory does not yield an indication for an isotropic-nematic phase transition, in contrast to HNC theory. The good quality of PY theory for *prolate* ellipsoids has been confirmed.[17,18] Particularly it has been demonstrated that reasonably good PY predictions require that terms up to $l_{max}=6$ are taken into account.[18] In variance with

[a)]URL: http://www.crs-soft.it; electronic mail: cristiano.demichele@phys.uniroma1.it

the observation of Ref. 15 it has been recently found that the PY theory also yields an isotropic-nematic phase transition.[19]

Finally we mention that the direct correlation functions $c_{ll'm}(r)$ obtained from a MC simulation[20] have been compared with the *Ansätze* described in Refs. 2 and 4–9. Some of them exhibit a satisfactory agreement with the MC results, particularly for large r values. But in our opinion the agreement is less good than the one found from integral equation theory.[15,17,18]

The above short review on previous investigations of hard ellipsoids makes it obvious that the debate on the orientational structural properties is not quite settled. Therefore, we have applied a newly developed event-driven MD algorithm[21] in order to calculate the static molecular correlation functions of hard ellipsoids in q space. In contrast to previous work described above, we have chosen the tensorial correlators $S_{\lambda\lambda'}(\mathbf{q})$, $\lambda=(l,m)$ (see Sec. II B). They have the advantage that they can directly be deduced from neutron and synchrotron radiation scattering experiments, at least for $l\leq2$. One of our main goals is to compare accurate numerical results with PY predictions from Ref. 8, obtained for the Gaussian overlap model[22] and with a truncation at $l_{max}=8$, a value larger than the one previously used in Ref. 18. Besides this, we will interpret the peak structure of these correlators, particularly of the nondiagonal one, $S_{2000}(\mathbf{q})$. We will demonstrate that the qualitative q dependence of this nondiagonal correlator allows us to easily distinguish between oblate and prolate ellipsoids. The application of first order thermodynamic perturbation theory for $S_{2000}(\mathbf{q})$ will provide support to this finding. Finally, we want to check how far the prediction of an isotropic-nematic phase transition[20] found from the growth of $S_{2020}(\mathbf{q}=0)$ is reproduced by our MD simulation.

The outline of the manuscript is as follows. In the next section we will describe the model and the tensorial functions $S_{\lambda\lambda'}(\mathbf{q})$. Section III contains results concerning (i) a comparison for $S_{\lambda\lambda'}(\mathbf{q})$ from PY theory and MD simulation, (ii) a geometrical interpretation of the q dependence of $S_{2000}(\mathbf{q})$, and (iii) the first order perturbation theory for $S_{\lambda\lambda'}(\mathbf{q})$. Section IV contains our conclusions.

II. METHODS

A. Model

We study a system composed of $N=256$ or 2048 uniaxial hard ellipsoids, i.e., ellipsoids with revolution axis of length a and two other axes of identical length b in a volume V. The aspect ratio is defined as $X_0 \equiv a/b$, with $0 < X_0 < \infty$. The volume of each particle is $\pi X_0 b^3/6$ and thus the packing fraction $\phi \equiv \pi X_0 b^3 \rho/6$ (where $\rho=N/V$ is the number density). We perform event-driven molecular dynamics simulations, with periodic boundary conditions, at several values of $0.4 < \phi < 0.51$ and several $0.4 < X_0 < 2.8$ values. Distances are measured in units of the axes geometric mean $l \equiv \sqrt[3]{ab^2}$. Ellipsoids have mass $m=1$ and a spherically symmetric momentum of inertia, i.e., $I_x=I_y=I_z=2mr^2/5$ with $r=\min\{a,b\}/2$.

The event-driven molecular dynamics simulation[21] for a one-component hard-ellipsoids system (HES) used in this work is described in details in Ref. 23. The prediction of
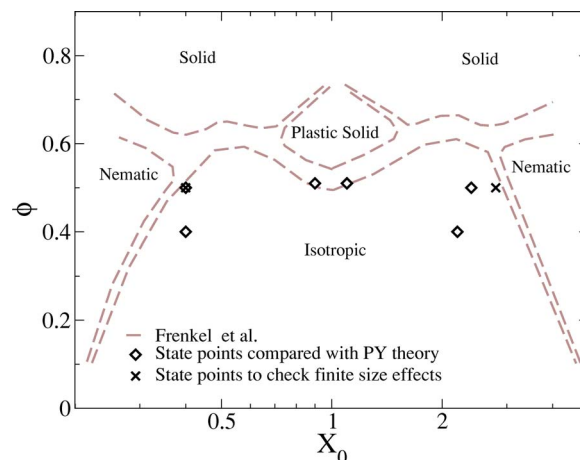

FIG. 1. Hard ellipsoids phase diagram. The dashed line are the phase boundaries calculated by Ref. 30. The open diamonds correspond to the points of the phase diagram which we compare with the PY results of Ref. 19. The X's correspond to the points of the phase diagram for which we have analized finite size effects.

events (collisions among molecules) is different from what has been proposed in the past. It relies on evaluations of distance between objects based on gradient descent and Newton-Raphson root finding algorithms. Such strategy in principle works for any objects whose surface is differentiable and hence it is not limited to ellipsoids. The efficiency of the algorithm is comparable to the algorithm recently proposed by Donev *et al.*[24]

To create the starting configuration, we generate a random configuration at very low ϕ and grow independently the particles up to the desired ϕ (i.e., we perform a quench in ϕ at fixed N, X_0). To equilibrate the systems, we simulate until the angular second Legendre polynomial correlation function, for the angle associated to the axis of symmetry, has decayed to zero. In addition we check that particles have diffused more than $\max\{a,b\}$. Simulations last approximately from 10^8 to 10^9 hard-ellipsoid collisions; between 1000 and 5000 equally spaced configurations have been stored for the analysis. Figure 1 shows the studied state points together with the known thermodynamic lines. The majority of the studied points lies close to the equilibrium transition line to maximize the structural signatures in the static correlation functions.

B. Molecular structure factors

A system of N rigid molecules can be described by the positions of the centers $\mathbf{r}_j$ and the orientation (Euler angles) $\mathbf{\Omega}_j$ of the jth molecule. The microscopic density $\rho(\mathbf{r},\mathbf{\Omega})=\Sigma_j\delta(\mathbf{r}-\mathbf{r}_j)\delta(\mathbf{\Omega}-\mathbf{\Omega}_j)$ can be expanded with respect to plane waves $e^{i\mathbf{q}\cdot\mathbf{r}}$ and to Wigner matrices $D_{mn}^{l*}(\mathbf{\Omega})$.[13,25] For molecules with a rotational symmetry axis, $\mathbf{\Omega}\equiv(\theta,\phi)$, Wigner matrices reduce to spherical harmonics and the microscopic density can be expanded into tensorial modes,

$$\rho_{lm}(\mathbf{q}) = \sqrt{4\pi}i^l\sum_{j=1}^{N} e^{i\mathbf{q}\cdot\mathbf{r}_j}Y_{lm}(\mathbf{\Omega}_j),$$

where l takes integer values ≥0 and m runs between $-l$ and l. The factor in front of the sum is for technical convenience.
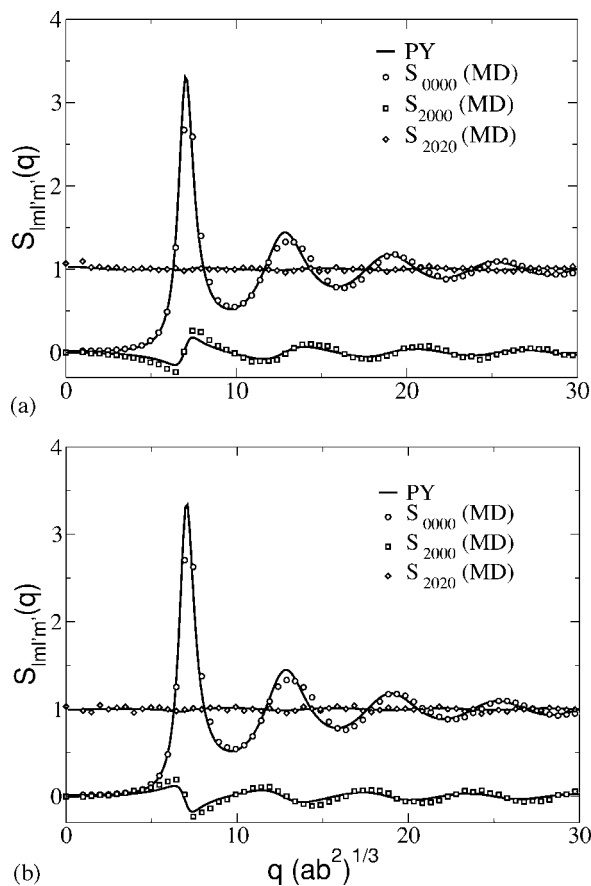
FIG. 2. $S_{lml'm'}(\mathbf{q})$ for $X_0=0.9$ (top) and $X_0=1.1$ (bottom) at $\phi=0.51$, i.e., near the hard-sphere case $X_0=1$. Symbols are simulation results, and the lines are PY predictions from Ref. 19.
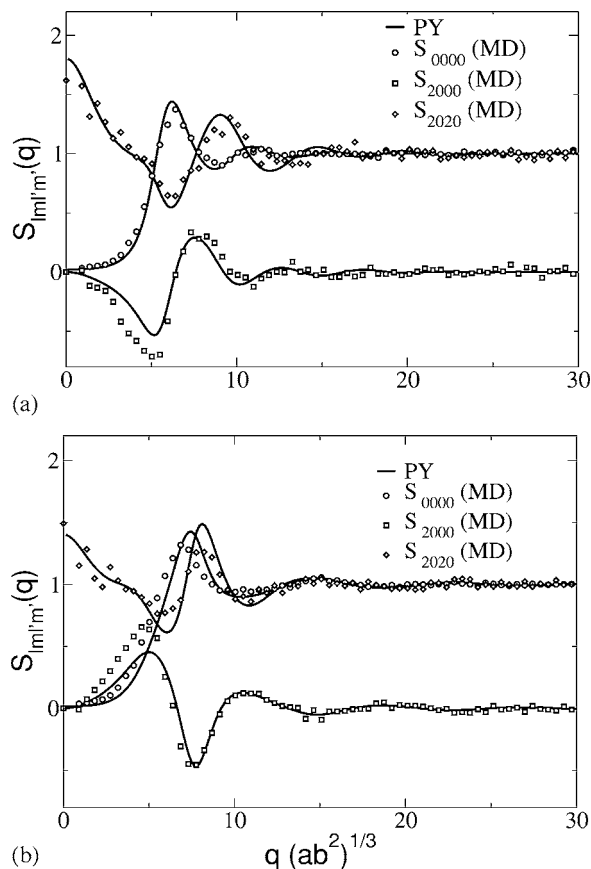

FIG. 3. $S_{lml'm'}(\mathbf{q})$ at $\phi=0.4$ for $X_0=0.4$ (top) and $X_0=2.2$ (bottom). The symbols are simulation results, and the lines are PY predictions from Ref. 19.

The molecular structure factors are defined as

$$S_{lml'm'}(\mathbf{q}) = \frac{1}{N}\langle \rho_{lm}^*(\mathbf{q})\rho_{l'm'}(\mathbf{q})\rangle$$

that will in general depend both on the modulus and on the orientation of $\mathbf{q}$. The symbol $\langle\cdots\rangle$ indicates an ensemble average. A convenient reference system is provided by the q frame, where the direction of the z axis is parallel to $\mathbf{q}$.[13] For molecules with a rotational symmetry axis, molecular structure factors in the q frame become diagonal in m (Ref. 26) so that $S_{lml'm'} = \delta_{mm'}S_{lml'm}$. For ellipsoids, the $S_{lml'm}(q)$ have been calculated within the Percus-Yevick approximation[19] and used as input of mode-coupling theory calculations to evaluate the glass transition lines.[27]

III. RESULTS AND DISCUSSION

A. Comparison between PY and simulation data for $S_{lml'm'}$

Figure 2 compares the numerical results and the PY predictions from Ref. 19 for S_{0000}, S_{2000}, and S_{2020} when $X_0 \approx 1$ (an almost hard-sphere case) for both oblate and prolate ellipsoids. In all cases, the PY predictions satisfactorily describe the numerical results. We note that S_{0000} resembles the typical shape of the HS fluid and is practically the same for oblate ($X_0=0.9$) and prolate ($X_0=1.1$) ellipsoids whereas S_{2020} is structureless for all q values (as expected since the

studied points are far from the nematic phase). Nevertheless, information on the angular structure are contained in S_{2000}. This function shows an interesting q behavior when comparing the prolate and oblate cases. Indeed, it appears that the prolate $S_{2000}(q)$ has an opposite sign as compared to the oblate one. We also notice that the location of the first peak of S_{0000} coincides with the location of one extremum also in the $S_{2000}(q)$.

Figure 3 shows data for the tensorial correlation functions for values deviating stronger from $X_0=1$, namely, $X_0=0.4$ and $X_0=2.2$ at $\phi=0.4$. Compared to the previous case, S_{0000} is less structured, while the opposite behavior is observed for both S_{2000} and S_{2020}. Even in this case, prolate and oblate ellipsoids are easily distinguished from the q dependence of S_{2000}: while for a prolate ellipsoids a maximum followed by a minimum is observed, the opposite behavior characterizes oblate ellipsoids. The location of the first peak of S_{0000} is now shifted as compared to the location of the $S_{2000}(q)$ extremum. It is also interesting to observe that now a peak at $q=0$ is present in S_{2020}, signaling the buildup of a finite nematic correlation length[27] on approaching the nematic transition.

As a further case for comparing simulation results and theoretical predictions, Fig. 4 shows $S_{lml'm}$ for $\phi=0.5$ and $X_0=0.4$ and 2.4. These state points are the closest points to the isotropic-nematic boundary for which PY predictions are available from Ref. 19. Even in this case, the PY results
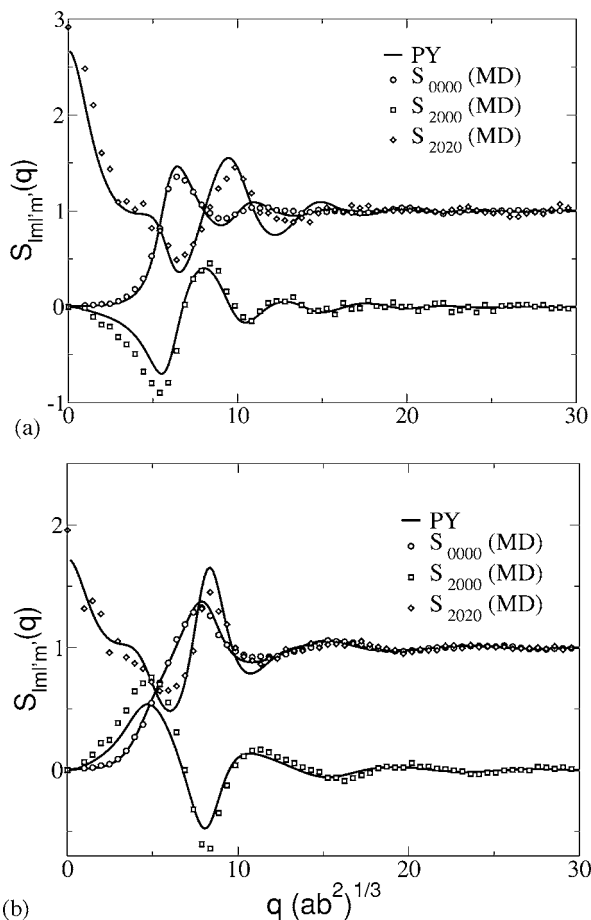
FIG. 4. $S_{lml'm'}(\mathbf{q})$ at values of ϕ near the nematic transition line, for values of X_0 corresponding to oblate/prolate ellipsoids; $X_0 = 0.4$, $\phi = 0.5$ (top) and $X_0 = 2.4$, $\phi = 0.5$ (bottom).

provide a satisfactory description of the q dependence. The growth of $S_{2020}(0)$ for $q \to 0$ at high/low elongations (Figs. 3 and 4) signals the presence of a growing correlation length ξ_{2020} for nematic order. If ξ_{2020} would be of the order of the box size, the results of our simulations would be affected by finite size effects. To test for the absence of such effects, we have simulated the two representative points $\phi = 0.50$, $X_0 = 0.40$, and $\phi = 0.50$, $X_0 = 2.80$ for $N = 2048$ ellipsoids. As shown in Figs. 5 and 6, the data for the biggest size are
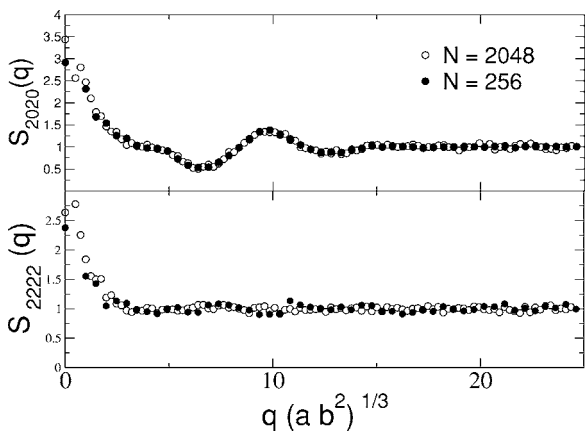

FIG. 5. Comparison of $S_{2020}(\mathbf{q})$ (top) and $S_{2222}(\mathbf{q})$ (bottom) for $N=256$ (full circles) and $N=2048$ (open circles) ellipsoids at $\phi=0.50$, $X_0=0.40$.
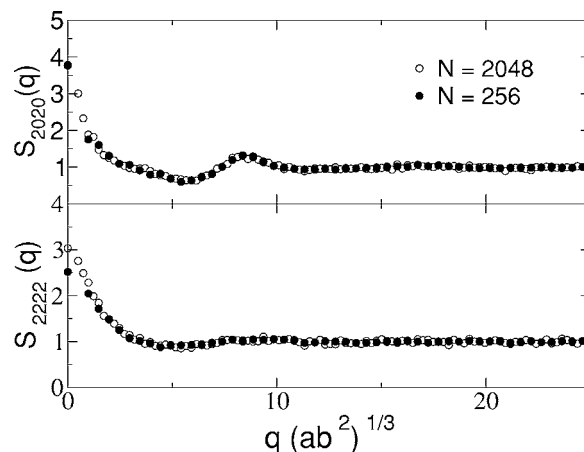

FIG. 6. Comparison of $S_{2020}(\mathbf{q})$ (top) and $S_{2222}(\mathbf{q})$ (bottom) for $N=256$ (full circles) and $N=2048$ (open circles) ellipsoids at $\phi=0.50$, $X_0=2.8$.

consistent with the results for the smaller size at lower q's, providing evidence of the absence of finite size effects in the studied state point. Additionally, Figs. 5 and 6 depict $S_{2222}(q)$ which has a pronounced peak at $q=0$, and which is almost structureless for larger q. We have also calculated correlators with l and/or l' equal to 4. Those are not shown, because they are of less experimental relevance. Nevertheless, we mention that they satisfactory agree with the PY result.

B. Geometrical characterization of the q dependence of S_{2000}

A hand-waving understanding of the antiphase character of the oblate/prolate S_{2000} function at same ϕ can be obtained by a geometrical analysis of the configurations. For the case of prolate particles ($X_0 > 1$), the location q^* of the first minimum in $S_{2000}(q)$ is located at $q^* \approx 2\pi/b$. At this small distance $r^* \approx b$, the two particles must be almost parallel. Since $\mathbf{q}$ is along the z axis (q frame) and the relative distance of the two particles has to be parallel to $\mathbf{q}$ in order to give a nonzero contribution to S_{2000}, the polar angle θ of both ellipsoids is close to $\pi/2$. This provides a negative contribution to S_{2000} because $Y_{20}(\theta, \phi) \equiv (3 \cos^2 \theta - 1)/2 \approx -1/2$ [Fig. 7(a)] assumes its smallest possible value. Hence, around q^*, where the majority of the pairs are parallel, S_{2000} will have a minimum. On the other hand, at the first maximum of S_{2000} ($q < q^*$) correlation between pairs of ellipsoids with relative distance $s^* \approx \max\{a, b\} > r^*$ is sampled. As we are working in the q frame, the pairs of ellipsoids at a distance s^* that will contribute to the maximum at q^* are those whose relative distance is parallel to $\mathbf{q}$. If we take into account the excluded volume effects due to the ellipsoids at distance $\approx r^*$, we see that the sterically favored configurations are the ones shown in Fig. 7(b). For such pairs of ellipsoids, the total contribution to S_{2000} in the q frame is positive. Therefore if we find an extremum at a distance $\approx s^*$ for prolate ellipsoids we expect that one to be positive.

The analysis of the configurations contributing to the peaks of S_{2000} for oblate ellipsoids is analogous. In the q frame there is a shift of $\pm \pi/2$ in θ. Therefore, the sign of Y_{20} is inverted and consequently the sign of S_{2000} is inverted with respect to the prolate case (see Fig. 8).
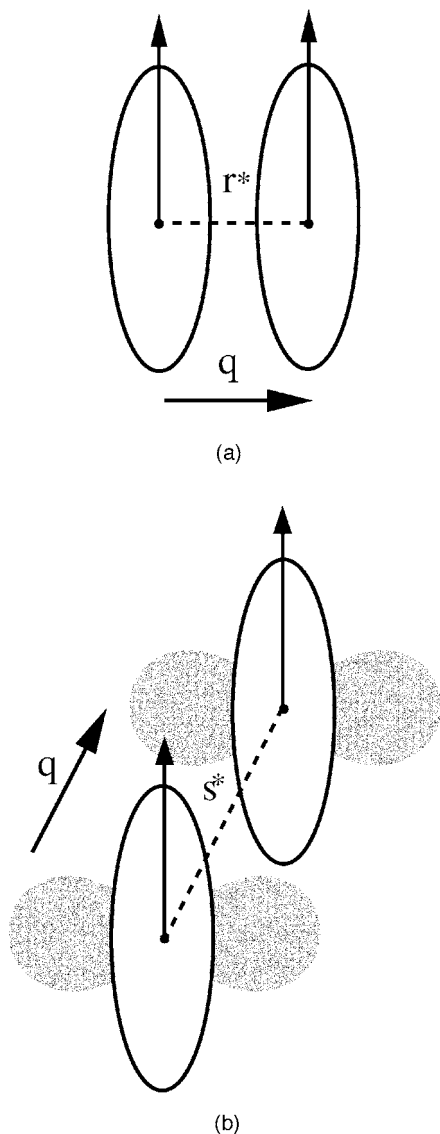
FIG. 7. (a) Sketch of configurations of two prolate ellipsoids with a center-to-center distance close to r^*. The values of Y_{20} in the q frame are negative for the two prolate ellipsoids because their rotational symmetry axes are almost perpendicular to q. (b) Configurations of ellipsoids with a center-to-center distance corresponding to s^*. The shaded region represents the volume excluded by particles at a distance $\sim r^*$. The values of Y_{20} in the q frame is positive because the rotational symmetry axes of both ellipsoids are almost parallel to **q**. The lines with the arrows placed on the ellipsoids centers represent the axes of symmetry of the ellipsoids.
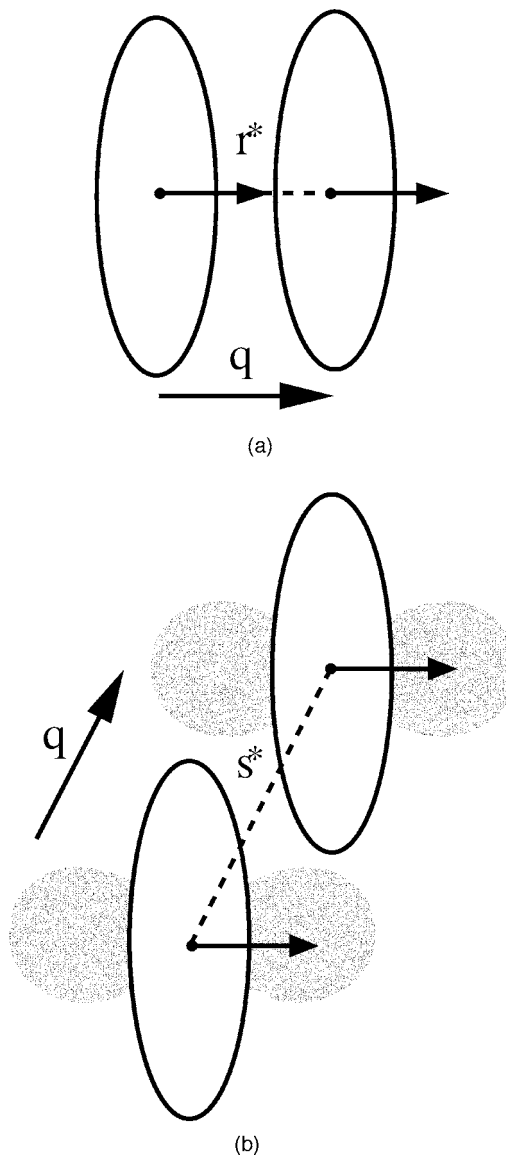

FIG. 8. (a) Sketch of configurations of two oblate ellipsoids with a center-to-center distance close to r^*. The values of Y_{20} in the q frame is positive for the two prolate ellipsoids because their rotational symmetry axes are almost parallel to q. (b) Configurations of ellipsoids with a center-to-center distance corresponding to s^*. The shaded region represents the volume excluded by particles at a distance $\sim r^*$. The values of Y_{20} in the q frame is negative for prolate ellipsoids because the rotational symmetry axes of both ellipsoids are almost perpendicular to **q**. The lines with the arrows placed on the ellipsoids centers represent the axes of symmetry of the ellipsoids.

C. First order perturbation theory for $S_{lml'm'}$

Specializing the results of Ref. 13 to hard ellipsoids, it is possible to expand the radial distribution function $g(\mathbf{r}_{12}, \mathbf{u}_1, \mathbf{u}_2)$ in a power series in $\varepsilon = X_0 - 1$,

$$g(\mathbf{r}_{12}, \mathbf{u}_1, \mathbf{u}_2) = \sum_{i=0}^{\infty} g_i(\mathbf{r}_{12}, \mathbf{u}_1, \mathbf{u}_2), \tag{1}$$

where $g_n = O(\varepsilon^n)$, $\mathbf{r}_{12}$ is the vector connecting two centers of the two ellipsoids, and $\mathbf{u}_i$ are the unit vectors along the rotational symmetry axes. The first two terms of the expansion are

$$g_0(\mathbf{r}_{12}, \mathbf{u}_1, \mathbf{u}_2) = g_{HS}(r_{12}), \tag{2}$$

$$g_1(\mathbf{r}_{12}, \mathbf{u}_1, \mathbf{u}_2) = -\bar{\sigma} g_{HS}(r_{12}) \gamma(\mathbf{u}_1, \mathbf{u}_2, \mathbf{e}_{12}) \delta(r_{12} - \bar{\sigma}) - \rho \bar{\sigma}$$

$$\times \int d^3 r_3 g_{HS}(\mathbf{r}_{12}, \mathbf{r}_{13}, \mathbf{r}_{23})$$

$$\times [\langle \gamma(\mathbf{u}_1, \mathbf{u}_3; \mathbf{e}_{13}) \rangle_{\mathbf{u}_3} \delta(r_{13} - \bar{\sigma})$$

$$+ \langle \gamma(\mathbf{u}_2, \mathbf{u}_3, \mathbf{e}_{23}) \rangle_{\mathbf{u}_3} \delta(r_{23} - \bar{\sigma})], \tag{3}$$

where $g_{HS}(r_{12})$ and $g_{HS}(\mathbf{r}_{12}, \mathbf{r}_{13}, \mathbf{r}_{23})$ are the static two-particle and three-particle distribution functions of hard spheres with effective diameter $\bar{\sigma}$ depending on ε, $\mathbf{r}_{ij} = r_{ij} \mathbf{e}_{ij}$, $\rho = N/V$ is the number density and

$$\langle f(\mathbf{u})\rangle_\mathbf{u} \equiv \frac{1}{4\pi}\int_0^{2\pi}d\varphi\int_0^\pi d\theta\,\sin(\theta)\,f(u(\theta,\psi)). \qquad (4)$$

The effective diameter $\bar{\sigma}$ is defined as $\bar{\sigma} = \langle\langle d(\mathbf{u}_1,\mathbf{u}_2,\mathbf{e}_{12})\rangle_{\mathbf{u}_1}\rangle_{\mathbf{u}_2}$, where $d(\mathbf{u}_1,\mathbf{u}_2,\mathbf{e}_{12})$ is the distance at contact of two ellipsoids with axis along $\mathbf{u}_i$ and $\mathbf{e}_{12}=\mathbf{r}_{12}/r_{12}$ is the direction between the centers of the ellipsoids. The function γ measures the "nonsphericity" of the potential and is defined self-consistently as $d(\mathbf{u}_1,\mathbf{u}_2,\mathbf{e}_{12})=\bar{\sigma}[1+\gamma(\mathbf{u}_1,\mathbf{u}_2,\mathbf{e}_{12})]$. At first order in ε, γ and $\bar{\sigma}$ can be evaluated analytically from geometrical considerations,

$$\bar{\sigma} = b\left[1+\frac{\varepsilon}{3}+O(\varepsilon^2)\right], \qquad (5)$$

$$\gamma(\mathbf{u}_1,\mathbf{u}_2,\mathbf{e}_{12}) = \frac{\varepsilon}{3}[P_2(\mathbf{e}_{12}\cdot\mathbf{u}_1)+P_2(\mathbf{e}_{12}\cdot\mathbf{u}_2)]+O(\varepsilon^2), \quad (6)$$

where P_l is the Legendre polynomial of order l.

The general expression of the molecular structure factor $S_{lml'm}$ in terms of $g(\mathbf{r}_{12},\mathbf{u}_1,\mathbf{u}_2)$ is
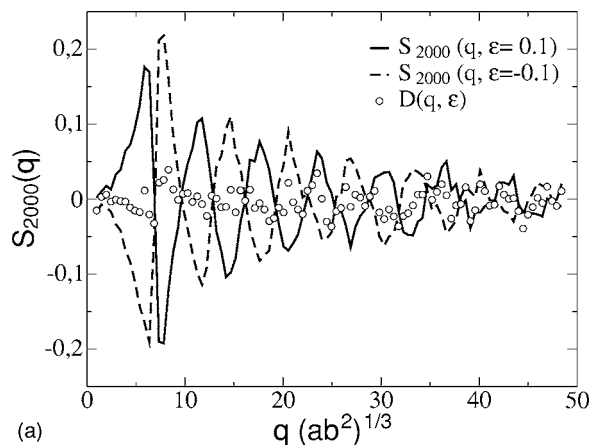
$$S_{lml'm}(\mathbf{q}) = \delta_{ll'}+i^{l'-l}\rho 4\pi$$
$$\times\int d^3r_{12}\langle\langle g(\mathbf{r}_{12},\mathbf{u}_1,\mathbf{u}_2)\cdot e^{i\mathbf{q}\cdot\mathbf{r}_{12}}$$
$$\times Y_{lm}^*(\mathbf{u}_1)Y_{l'm}(\mathbf{u}_2)\rangle_{\mathbf{u}_1}\rangle_{\mathbf{u}_2}. \qquad (7)$$

Using the properties of Legendre polynomials, we have that $\langle\gamma(\mathbf{u},\mathbf{w},\mathbf{e})\rangle_\mathbf{w}=(\varepsilon/3)P_2(\mathbf{e}\cdot\mathbf{u})$, so we can rewrite g up to first order,
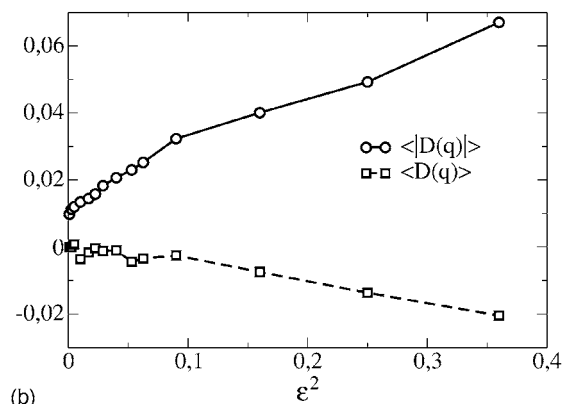
$$g(\mathbf{r}_{12},\mathbf{u}_1,\mathbf{u}_2)$$
$$= g_{HS}(\mathbf{r}_{12})-\frac{\epsilon\bar{\sigma}}{3}\Bigg\{g_{HS}(\bar{\sigma})[P_2(\mathbf{u}_1\cdot\mathbf{e}_{12})+P_2(\mathbf{u}_2\cdot\mathbf{e}_{12})]$$
$$\times\delta(r_{12}-\bar{\sigma})+\rho\int d^3r_3 g_{HS}(\mathbf{r}_{12},\mathbf{r}_{23},\mathbf{r}_{13})$$
$$\times[\delta(r_{13}-\bar{\sigma})P_2(\mathbf{u}_1\cdot\mathbf{e}_{13})+\delta(r_{23}-\bar{\sigma})P_2(\mathbf{u}_2\cdot\mathbf{e}_{23})]\Bigg\}. \qquad (8)$$

The zeroth order g_0 is spherically symmetric and will contribute with a diagonal term S_{lmlm}^0. The first order term contains functions of the form $P_2(\mathbf{u}_i\cdot\mathbf{e}_{ij})$ that can be recasted in terms of linear combinations of spherical harmonics $Y_{lm}(\mathbf{u}_i)$ with $l=0,2$; so the first order term will contribute only to $S_{lml'm}$ with $l,l'=0,2$ and $l\neq l'$.

In particular, in the q frame the ρ independent part of g_1 contains only linear combinations of Y_{00} and Y_{20}; it is then possible to evaluate $S_{lml'm}$ with the result,

FIG. 9. Check of Eq. (10) for the case $\phi=0.49$. The upper panel shows $S_{2000}(q)$ for $X_0=1\pm\epsilon$ and $D(q,\epsilon)$ for $\epsilon=0.10$. The lower panel shows the average of $|D(q,\epsilon)|$ (empty circles) over all $q<50$ from the simulation as a function of ϵ^2 for several values of ϵ. The behavior at low ϵ is linear in ϵ^2 as predicted from the first order perturbation theory. The presence of a constant term in $\langle|D(q,\epsilon)|\rangle$ for $\epsilon\to0$ is due to the noise implicit in the measures. In fact, the values $\langle D(q,\epsilon)\rangle$ (empty squares) at small ϵ are dominated by the noise and are scattered around zero. The ϵ^2 regime seems to break down around $\epsilon\sim0.3$.

$$S_{lml'm}(q,\epsilon)$$
$$= \delta_{ll'}S_{lmlm}^0(q)-\epsilon\frac{2\pi}{3\sqrt{5}}\rho\bar{\sigma}^3 g_{HS}(\bar{\sigma})$$
$$\times[(x^{-1}-2x^{-3})\sin x+2x^{-2}\cos x]$$
$$\times[\delta_{lm,20}\delta_{l'm,00}+\delta_{lm,00}\delta_{l'm,20}]+\rho\varepsilon\mathcal{F}_{lml'm}(\bar{\sigma})+O(\varepsilon^2), \qquad (9)$$

where $x=|q|\bar{\sigma}$ and $\mathcal{F}_{lml'm}(\bar{\sigma})$ is a function of $\bar{\sigma}$ that does not depend on ε. Its calculation requires the knowledge of the static three-point correlator $g_{HS}(\mathbf{r}_{12},\mathbf{r}_{13},\mathbf{r}_{23})$, which, however, is not known exactly.

Therefore, S_{2000} shows a peak of opposite sign around $q\sim\bar{\sigma}^{-1}$ as observed above when discussing the simulation data; in general, first order theory predicts

$$D(q,\epsilon) = S_{2000}(q,\epsilon)+S_{2000}(q,-\epsilon)=0, \qquad (10)$$

for ε small enough. We check this last property by our simulations. Figure 9 (top) shows $S_{2000}(q,\epsilon)$, $S_{2000}(q,-\epsilon)$, and $D(q,\epsilon)$ for $\varepsilon=0.05$. The sum $D(q,\epsilon)$ vanishes within the error, supporting the prediction of Eq. (10). To gather a feel-

ing of the range of validity of this prediction we show in Fig. 9 (bottom) the average value (over all $q < 50$) of $|D(q, \epsilon)|$ and $D(q, \epsilon)$ as a function of ϵ^2. The behavior of $\langle D(q, \epsilon) \rangle$ and $\langle |D(q, \epsilon)| \rangle$ confirms the linear dependence on ϵ^2 predicted from Eq. (10) for $\epsilon \lesssim 0.1$.

IV. CONCLUSIONS

In this paper we have presented a comparison between PY predictions and MD simulation results for the tensorial correlators in a hard ellipsoids liquid, close to the phase coexistence lines.

The major focus has been on the calculation of static molecular correlation functions. In contrast to earlier work we have not chosen the r-dependent coefficients $g_{ll'm}(r)$ of an expansion with respect to rotational invariants but the tensorial correlators $S_{lml'm'}(\mathbf{q})$ in q space. Those have the advantage that they can be obtained from scattering experiments, at least for $l, l' \leq 2$. The comparison of the correlators from MD simulations with the corresponding ones from the PY theory[19] is rather satisfactory for all correlators and all pairs of (X_0, ϕ) we have studied. Accordingly, the good agreement between results from the PY theory and an earlier MD simulation found in Ref. 18 is confirmed. An interesting observation made is the qualitative difference of the nondiagonal correlator $S_{2000}(q)$ for oblate and prolate shapes. Since the back transform to real space is a linear procedure, this qualitative different behavior should also exist for $G_{2000}(r)$ which is related to the coefficient $g_{200}(r)$. Indeed, Fig. 1(a) for $X_0 = 2$ and Fig. 4 for $X_0 = 1/3$ from Ref. 15 show that the first extremum of $g_{200}(r)$ is a minimum and a maximum, respectively.

The qualitative shape dependence of $S_{2000}(q)$ has been proven analytically. Using the first order perturbation theory with respect to $\varepsilon = X_0 - 1$ we have shown that $S_{2000}(q)|_{\text{prolate}} \approx -S_{2000}(q)|_{\text{oblate}}$.

We have not attempted to compare $S_{2000}(q)$ from this perturbational approach, with the corresponding result from our MD simulation and PY theory, because one needs the static three-point correlator for hard spheres as an input which is not known.

It has recently been predicted[28] that the time-dependent correlator $S_{2000}(\mathbf{q}, t)$, which is a measure of the coupling between the center of mass ($l = 0$) and orientational ("quadrupolar" part $l = 2$) motion, has an effect on the light scattering spectra. This effect has been found experimentally[29] and might offer the possibility to check how far spectra from light scattering experiments may allow to discriminate between oblate and prolate particles.

Finally, we have checked the growth of nematic order. In contrast to the PY result in Ref. 14 the authors of Ref. 19 have found that $S_{2020}(q = 0)$ from PY theory diverges at a critical volume fraction $\phi_c(X_0)$ for $X_0 \gtrsim 2$ and $X_0 \lesssim 0.5$. At ϕ_c an isotropic-nematic transition occurs. Our simulation reproduces the shape and the growth of the peak of $S_{2020}(q)$ at low q's. We have also demonstrated that, for the chosen values of X_0 and ϕ, no finite size effects influences this peak. We have

not attempted to determine $\phi_c(X_0)$ from our simulation since this type of analysis would request much larger system sizes than we are currently able to simulate.

The PY tensorial correlators have been recently used as input in molecular mode-coupling theory to evaluate the glass lines in the $(X_0 - \phi)$ plane. The theoretical calculations suggest the possibility of a new mechanism of slowing down of the dynamics driven by the increase of the nematic order. Therefore, the validity of the PY predictions, particularly for the peak of S_{2020} close to $q = 0$, presented in this work confirms that this new mechanism is not arising from a failure of the PY predictions, but it is a genuine prediction of the molecular mode-coupling approach.

[1] J. P. Hansen and I. R. McDonald, *Theory of Simple Liquids* 2nd ed.(Academic, New York, 1986).
[2] R. Pynn, Solid State Commun. **14**, 29 (1974).
[3] R. Pynn, J. Chem. Phys. **60**, 4579 (1974).
[4] A. Wulf, J. Chem. Phys. **67**, 2254 (1977).
[5] J. D. Parsons, Phys. Rev. A **19**, 1225 (1979).
[6] S. D. Lee, J. Chem. Phys. **87**, 4972 (1987).
[7] S. D. Lee, J. Chem. Phys. **89**, 7036 (1987).
[8] M. Baus, J.-L. Colot, X.-G. Wu, and H. Xu, Phys. Rev. Lett. **59**, 2184 (1987).
[9] J. F. Marko, Phys. Rev. A **39**, 2050 (1989).
[10] A. Chamoux and A. Perera, J. Chem. Phys. **104**, 1493 (1996).
[11] A. Chamoux and A. Perera, Mol. Phys. **93**, 649 (1998).
[12] G. Rickayzen, Mol. Phys. **95**, 393 (1998).
[13] C. G. Gray and K. E. Gubbins, *Theory of Molecular Fluids* (Clarendon, Oxford, 1984, Vol. 1).
[14] A. Perera, P. G. Kusalik, and G. N. Patey, J. Chem. Phys. **87**, 1295 (1987).
[15] J. Talbot, A. Perera, and G. N. Patey, Mol. Phys. **70**, 285 (1990).
[16] J. W. Perram, J. L. M. S. Wertheim, and C. O. Williams, Chem. Phys. Lett. **105**, 277 (1984).
[17] J. Ram and Y. Singh, Phys. Rev. A **44**, 3718 (1991).
[18] J. Ram, R. C. Singh, and Y. Singh, Phys. Rev. E **49**, 5117 (1994).
[19] M. Letz and A. Latz, Phys. Rev. E **60**, 5865 (1999).
[20] M. P. Allen, P. Mason, E. de Miguel, and J. Stelzer, Phys. Rev. E **52**, R25 (1995).
[21] D. C. Rapaport, *The Art of Molecular Dynamics Simulation* (Cambridge University Press, Cambridge, 2004).
[22] B. J. Berne and P. Pechukas, J. Chem. Phys. **56**, 4213 (1972).
[23] C. De Michele and A. Scala (unpublished).
[24] A. Donev, F. H. Stillinger, and S. Torquato, J. Comput. Phys. **202**, 737 (2005).
[25] L. Fabbian, A. Latz, R. Schilling, F. Sciortino, P. Tartaglia, and C. Theis, Phys. Rev. E **62**, 2388 (2000).
[26] R. Schilling and T. Scheidsteger, Phys. Rev. E **56**, 2932 (1997).
[27] M. Letz, R. Schilling, and A. Latz, Phys. Rev. E **62**, 5173 (2000).
[28] T. Franosch, A. Latz, and R. M. Pick, Eur. Phys. J. B **31**, 229 (2003).
[29] H. P. Zhang, A. Brodin, H. C. Barshilia, G. Q. Shen, H. Z. Cummins, and R. M. Pick, Phys. Rev. E **70**, 011502 (2004).
[30] D. Frenkel, B. M. Mulder, and J. P. McTague, Phys. Rev. Lett. **52**, 287 (1984).